参赛队员姓名：佘悦杭

中学：深圳中学

省份：广东省

国家/地区：中华人民共和国

指导教师姓名：赵若

指导教师单位：南方科技大学前沿与交叉科学研究院

论文题目：纤维增强型复合聚合物电解质的制备及其在全固态电池中的应用

Synthesis of fiber-reinforced composite polymer electrolyte for high-performance solid-state batteries

Abstract

All-solid-state Li-ion battery is the next-generation energy storage device to meet the ever-growing demand for energy. As one of the key components, solid-state electrolyte plays an important role in determining battery performance. Solid polymer electrolytes (SPEs) are attractive due to their high flexibility and easy processability. However, SPEs suffer from low ionic conductivity and poor mechanical stability. The design and addition of nanostructured solid fillers are an effective way to optimize the SPEs' properties. In this work, a three-dimensional fibrous membrane composed of metal-organic frameworks (MOFs) is produced and used as the functional filler to prepare fiber-reinforced SPE. The MOF-incorporated fiber enables sufficient contact with the polymer matrix of SPE and can selectively immobilize anions via a pore confinement effect. Additionally, MOF with rich porosity and ordered channels can regulate a uniform Li^+ distribution in the electrolyte/electrode interface, which can suppress the growth of Li dendrites and improve interfacial stability. The as-assembled symmetrical battery can stably run for 500 h with small polarization. The Li | $LiFePO_4$ full cell delivers a high capacity of 127 mAh g^{-1} at 1 C after 500 cycles. This work verifies the effectiveness of MOF-incorporated fibrous fillers in producing high-performance electrolytes for solid batteries.

Keywords: solid-state battery; solid polymer electrolyte; solid filler; metal-organic framework; three-dimensional fibers; ionic conductivity.

1. INTRODUCTION

As one of the representative energy storage devices, Li-metal batteries (LMBs) have been widely used in many aspects of our modern society.[1] Nowadays, with the rapid development and increasing need for electric vehicles, the development of advanced LMBs with higher energy/power density and operating safety is required.[2] Conventional LMBs usually use organic liquid electrolytes, which are composed of lithium salts, organic solvents and other additives. However, the liquid electrolytes inside the batteries are corrosive, inflammable and explosive; once leaked, they will cause serious combustion and explosion accidents, and cause great harm to personal safety and property safety.

In hope of conquering the defects of liquid batteries, all-solid-state batteries (ASSBs), consisting of metallic Li anodes and solid-state electrolytes (SSEs), are researched and developed. Compared to liquid batteries, both security and performance have been improved in ASSBs. The utility of SSEs completely avoids the problems of flammability, explosion and leakage due to their solid phase. Additionally, SSEs can reduce the chance of short circuit, and can provide a higher mechanical property, thus greatly improving the operation safety.[3] In ASSEs, the use of Li metal anode in ASSBs has great advantages. Li metal possesses high theoretical specific capacity (3860 mAh g^{-1}) and low redox potential (-3.14 V vs. RHE), which can offer an increase of up to 70% in energy density.[4] Compared with liquid electrolyte, SSEs with high mechanical

strength can somewhat suppress the growth of Li dendrites and enhance the cycling stability. Thus, SSEs are expected to the development of high-performance ASSBs.

The SSEs mainly consist of two categories: inorganic solid electrolytes and solid polymer electrolytes (SPEs). Inorganic solid electrodes, for instance, oxides and sulfides, although usually having high ionic conductivity, suffer from fragility, air instability, and large interfacial impedance.[5] SPEs, like poly(ethylene oxide) (PEO)-based type, promise lightweight, high flexibility, and low interfacial impedance, while their low ionic conductivity and poor mechanical strength restrain their practical applications.[6] For the time being, PEO-based polymer electrolyte is faced with the disadvantages of low ionic conductivity at room temperature, low mechanical strength and low Li-ion migration number. The introduction of solid fillers can be an effective way to optimize the SPEs' overall performance. There are many merits of adding solid fillers: first of all, solid fillers can interact with PEO and increase the amorphous region, thus reducing the crystallization area. This can enhance the segmental motion of polymer chains and thus increase the Li^+ conductivity. Secondly, adding solid fillers can improve the mechanical properties of SSEs. Moreover, when the solid fillers can selectively immobilize anions, a much higher Li^+ transference number could be achieved. In this condition, a more uniform Li deposition process and a more stable interface between electrolyte and electrode could be obtained, which will improve the durability and stability of batteries.

The conventional solid fillers (e.g., SiO_2, Al_2O_3, TiO_2, etc.) exhibit an ability to improve the performance of SPEs. However, these materials still suffer from the

problem of having low specific surface area and poor surface polarity, which causes the low interaction strength with polymers and Li salts. Thus the improvement in battery performance is limited.[5] In recent years, metal-organic frameworks (MOFs) start being applied to SSEs as solid fillers. There are many merits of using MOF as solid fillers: first of all, MOF possesses a very high surface area, which means that the interaction with other components is more sufficient, optimizing the electrochemical performances of SPEs. The high surface area also renders MOFs to have high absorption ability, which enables it to capture and trap the impurities or by-products and thus suppress the side reactions. Besides, the rich porosity of MOFs offers uniformly dispersed sites and clear paths for ion diffusion, showing great advantages over conventional solid fillers.[7] Current works done on MOF-incorporated SPEs mainly focus on the direct suspension of MOF nanoparticles within polymeric matrix. One prominent obstacle is that agglomeration occurs frequently between MOF nanoparticles, and thus reduces the internal contact and interactions. In order to eliminate the occurrence of agglomeration between MOF nanoparticles as much as possible, constructing three-dimensional (3D) MOF fibers as solid fillers is effective and promising.

In this work, a three-dimensional (3D) MOF-incorporated fiber (denoted as MF) was prepared by an electrospinning method. After casting LiTFSI/polyethylene oxide (PEO) (denoted as LP) within the MF membrane, a fiber-reinforced SPE (denoted as MF@LP) was obtained. The synthesis process is illustrated in **Scheme 1**. Thanks to the intrinsic characteristics of MOF (high surface area, rich surface polarity, cage-like pores, ordered channels, etc.), the MF as solid filler can generate a full contact with LP,

interacted with the ether oxygen groups in PEO, and selectively immobilize the movement of $TFSI^-$ anions. Consequently, the MF@LP electrolyte demonstrated a high ionic conductivity, good stability and excellent stability when assembled into batteries. In Li | MF@LP | Li symmetrical cell, a small polarization of 0.09 mV can be maintained after cycling for 500 h. In Li | MF@LP | $LiFePO_4$ full cell, a high specific capacity of 160 mAh g^{-1} was obtained, which was slightly decreased to 127 mAh g^{-1} after 500 cycles. The excellent battery performance proves that the obtained MF@LP is a promising electrolyte that not only enables a fast Li^+ migration, but also a uniform Li deposition.

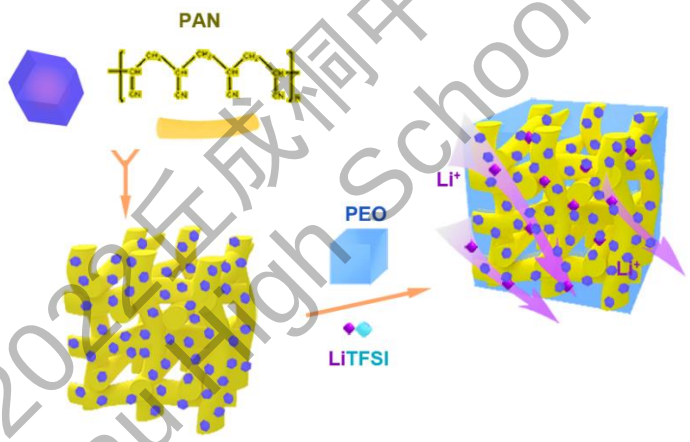

Scheme 1. The schematic illustration of preparation of MOF-incorporated fiber and fiber-reinforced SPE.

2. EXPERIMENTAL DETAILS

2.1 Synthesis of MOF nanoparticle

First of all, dissolve 1.436 g of $Co(NO_3)_2 \cdot 6H_2O$ and 3.244 g of 2-methylimidazole respectively into 100 mL of methanol each, under an ambient temperature of 25 °C.

Then pour the former salt solution into the latter ligand solution under vigorous stirring, and continue to stir the solution for 12 min. After the mixture being kept for 20 h to ensure sufficient reaction, a centrifugation method is used to separate the solid products from the mixture. the obtained ZIF-67 nanoparticles are then washed with methanol for 3 times, and vacuum-dried at 150 ºC for 8 h.

2.2 Preparation of MOF-incorporated fibers

Dissolving 0.3 g polyacrylonitrile (PAN) into 2.8 mL of N, N-dimethylformamide (DMF), and then adding 0.3 g ZIF-67 nanoparticles to the obtained solution. Leave the mixture overnight for magnetic stirring in order to ensure that it is well-mixed, so that the ZIF-67 nanoparticles are uniformly dispersed, which is related to the subsequent electrospinning procedure. During electrospinning, apply a high voltage of 15 kV to the solution, which is contained in a syringe and spun out through the needle to form nanofibers. The spun nanofibers are collected on a copper foil placed 15 cm away from the needle, thus forming a fibrous membrane. After removing and collecting the fibrous membranes from the copper foil, dry them in vacuum ovens at 80 ºC for 2 h in order to ensure that no residual organic solvents exist. Store the ultimately obtained sample in a glove box (H_2O < 0.01 ppm, O_2 < 0.01 ppm), in order to prevent the negative influence of water and oxygen in the air.

2.3 Preparation of SPEs

The 3D MOF-incorporated fibers (denoted as MF) have been prepared and applied as solid filler to construct fiber-reinforced SPE (denoted as MF@LP) as shown in **Scheme**

1. First of all, add 2 g of PEO (molecular weight ~ 300000) and 0.8 g of LiTFSI into 16 mL of acetonitrile, then stir the mixture for 3 h at room temperature, acquiring a uniform solution PEO/LiTFSI (denoted as LP). To get rid of the bubbles in the solution, a treatment using the planetary centrifugal paste mixer (Thinky SR-500) is applied. After that, cast the LP solution into the FM membranes, then dry them at 80 ºC for 16 h.

To investigate the effects of MOFs and the 3D fibrous structure, controlled samples, including MOF-free SPEs (denoted as PAN@LP) and MOF nanoparticle-incorporated SPEs (denoted as MP@LP) were also synthesized. The synthesis procedure of PAN@LP was similar to that of MF@LP except that on MOF was added to the system. To prepare MP@LP, 2 g of PEO (molecular weight ~ 300000), 0.8 g of LiTFSI and 0.14 g ZIF-67 nanoparticles were mixed in acetonitrile. The as-obtained slurry was casted on a PTFE and was dried at 80 ºC to form the free-standing membrane. The content of ZIF-67 in MP@LP was the same with that in MF@LP, so that the advances of the 3D fibrous structure could be studied. All the procedures were done in a glove box (H_2O < 0.01 ppm, O_2 < 0.01 ppm).

2.4 Material characterizations

In order to examine the crystalline phase of the material, a X-ray diffraction (XRD) method of Cu Kα radiation (λ = 1.5418 Å) was applied to the sample. Using the scanning electron microscopy (SEM) approach, we investigated the surface and cross-sectional morphology of the materials. Differential scanning calorimetry (DSC) was performed to detect the melting point of the electrolytes with a ramp rate of 5°C min^{-1}.

2.5 Preparation of the electrodes

The cathode was made by a slurry casting method on a basal carbon-coated aluminum foil. The slurry was synthesized by mixing the commercial $LiFePO_4$ (LFP) power, super P, polyvinylidene difluoride (PVDF), and LiTFSI in N-methyl-2-pyrrolidone (NMP) with a weight ratio of 60 : 12 : 20 : 8 : 360. The slurry was casted to the carbon-coated aluminum foil using a doctor blade method, and then dried overnight in a vacuum oven at 80℃. The active mass loading of LFP was 2 mg cm^{-2}.

2.6 Electrochemical measurements

The as-synthesized SPEs were assembled into batteries in a Ar-filled glove box in a standard 2032 coin-cell configuration. The ionic conductivity (σ) was measured by a electrochemical impedance spectroscopy (EIS) method. Two stainless-steel (SS) blocking electrolytes were placed on the two sides of the SPEs. The σ can be measured in the frequency range of 0.1-10^6 Hz between 25 and 60 ºC with an amplitude of 10 mV, and calculated using equation (1) below:

$$\sigma = d /(S \times R) \qquad (1)$$

Where d represents the thickness, S is the surfaced area and R is the resistance of SPEs. The electrochemical stability was tested by a linear sweep voltammetry (LSV) method. The electrodes in the battery in LSV testing are the stainless-steel and a Li foil. The voltage range was from 3 to 6 V with a scan rate of 0.5 mV s^{-1}. The performance of Li | SPEs | Li symmetrical cells and Li | SPEs | LFP full cells were evaluated by

galvanostatic charge-discharge method at 60 °C. The current density in symmetrical cells was set as 0.3 mA cm^{-2}. The cut-off voltage in full cells was set from 2.9 to 3.8 V.

3. RESULTS AND DISCUSSION

3.1. Material characterization

Fig. 1a illustrates the structure of ZIF-67 crystal. Each Co ion is coordinated with 4 ligands, which are periodically connected to form a network structure. By an electrospinning technology, ZIF-67 nanoparticles (denoted as MP) and PAN are integrated into fibers (denoted as MF). **Fig. 1b** illustrates the XRD results of MF and MP, which correspond well to the peaks of the simulated one. It proves the successful synthesis of ZIF-67 with high crystallinity. ZIF-67 demonstrates a dodecahedron-shaped morphology with an average size of around 260 nm, as shown in **Fig 1c**. The MF membrane has a fibrous structure, on which ZIF-67 nanoparticles are densely distributed (**Fig. 1d** and **Fig. 1e**). The diameter of the fiber is relatively uniform at around 1 μm. The well dispersion of ZIF-67 nanoparticles on MF can effectively prevent their agglomeration and thus favors a good and stable functionality. After infiltrating LiTFSI/PEO (LP) within MF, the fiber-reinforced MF@LP SPE is produced. **Fig. 1f** shows the surface morphology of MF@LP, which is flat and smooth without cracks or holes. The flexible surface will benefit the process of Li plating and stripping, which may stabilize the interfacial contact with electrodes.

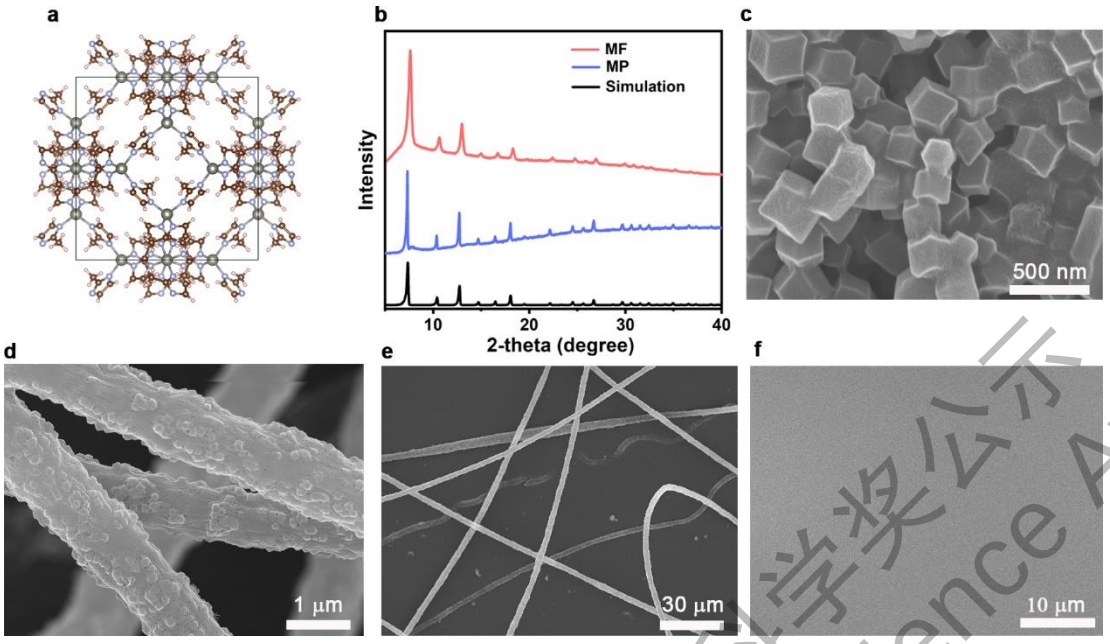

Figure 1. (a) The topology and coordination environment of ZIF-67. (b) The XRD patterns of MF, MP, and the simulated one. (c) The SEM image of MP. (d) and (e) The SEM image of the MF under different magnifications. (f) The SEM image of the surface morphology of MF@LP.

3.2. Electrochemical performance of material ZIF-67

Fig. 2a shows the thermogravimetric analysis (TGA) curves of MF@LP and MP@LP. It should be noted that almost no mass loss occurred before 280 ºC, indicating that there is hardly any residual organic solvent in the samples. Thus, the as-obtained SPEs in this study has high safety. The differential scanning calorimetry (DSC) measurement is conducted on MF@LP, MP@LP, and LP to investigate the influence of MOF addition and 3D fibrous structure on the PEO matrix (**Fig.2b**). The endothermic peaks in DSC curves correspond to the melting temperature of PEO matrix, which reflex the amorphous degree of the PEO. Compared with LP, MF@LP and MP@LP exhibit a much lower melting temperature. It proves that the introduction of MF and MP is

effective to decrease the PEO's crystallinity and thus enhance the PEO chains' mobility. The faster segmental mobility of polymer chains can favor Li^+ migration by providing rich hopping sites. The melting temperatures of MF@LP and MP@LP are similar, suggesting that there is little difference between MF and MP in affecting the PEO's amorphous state. This was reasonable since the fibrous structure are useful in preventing particle agglomeration rather than improving the interactions with PEO matrix. The improvement in PEO's chains and Li^+ mobility will be reflected in the SPEs' ionic conductivity, which will be discussed later.

The electrochemical window is a vial factor for SPEs since it determines their compatibility with high-voltage cathodes. As shown in **Fig. 2c**, the linear sweep voltammetry (LSV) curve of MF@LP displays a potential window of approximately 4.2 V, which is much higher than the previously reported PEO-based SPEs. The improvement could be attributed to the stabilization effect on the ether oxygen of PEO by the added fillers (MF or MP).

Figs. 2d, 2e and **2f** are the results of electrochemical impedance spectroscopy (EIS) of sample MP@LP and MF@LP. The intersection of the semicircular arc and the lateral axis is used to calculate the resistance. By comparison, it can be found that MF@LP has the highest ionic conductivity of 6.09×10^{-6} S cm^{-1}, which is higher than those of MP@LP (5.06×10^{-6} S cm^{-1}) and LP (3.73×10^{-6} S cm^{-1}) at room temperature. The superior conductivity of MF@LP and MP@LP over LP is due to the existence of MF and MP fillers, which bring rich hopping sites for Li^+ migration. The ionic conductivities of MF@LP and MP@LP are similar, which is in agreement with the DSC

results. With the increase of testing temperatures, the ionic conductivity of SPEs increases significantly. At 60 ºC, MF@LP has a high ionic conductivity of 3 × 10^{-4} S cm^{-1}, respectively, which meets the criteria for battery utility.

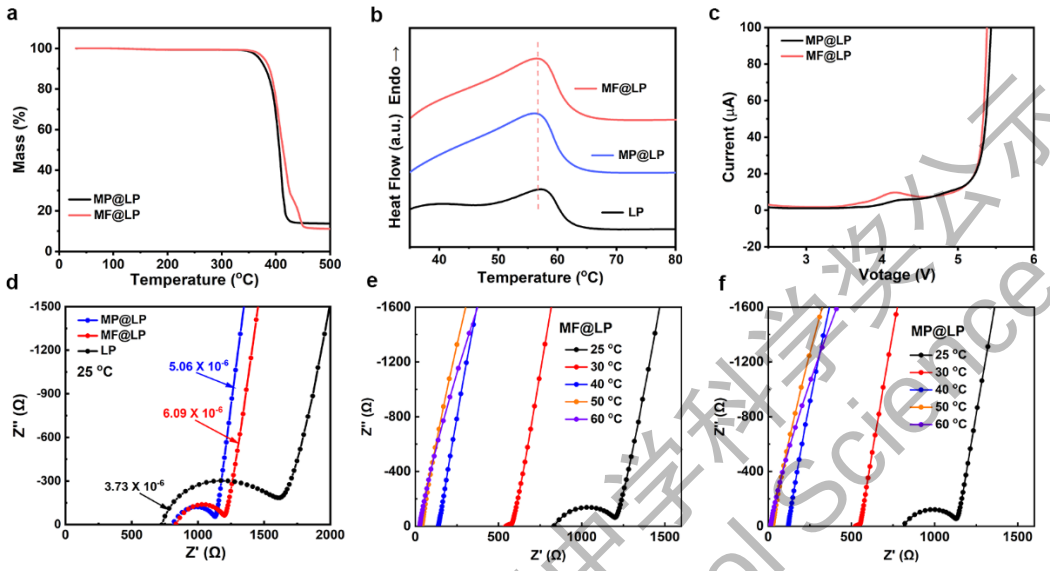

Figure 2. (a) The TGA curve of MP@LP and MF@LP. (b) The DSC curve of MF@LP, MP@LP, and LP. (c) The LSV curve of MP@LP and MF@LP. (d) The Nyquist plots of LP, MP@LP and MF@LP at 25 ºC. (e) The Nyquist plots of MF@LP at different temperatures. (f) The Nyquist plots of MP@LP at different temperatures.

3.3. Electrochemical performance of batteries

To investigate the compatibility of MF@LP and MP@LP with Li anodes, Li symmetrical cells are assembled and evaluated by galvanostatic charge-discharge method. As shown in **Fig. 3c**, the Li|MF@LP|Li battery can stably run for more than 500 h with the current density of 0.3 mA cm^{-2} at 60 ºC. In comparison, the Li|MP@LP|Li battery undergoes a short circuit after 60 h, which can be ascribed to Li dendrite growth and penetration. The ultralong cycling stability of Li|MF@LP|Li verifies the effectiveness of 3D fibrous structure in stabilizing the interface with

electrodes. Benefiting from the densely dispersed ZIF-67 nanoparticles, the 3D fibrous skeleton, and the rich -CN/NH_2 groups on MF, the MF@LP SPE enables a fast Li^+ migration, a uniform Li deposition and a stable internal condition near the SPE/electrolyte interface. All these characteristics lead to a suppression on Li dendrite growth and finally endow Li|MF@LP|Li cell with long-term cycling performance. Both the Li|MP@LP|Li and Li|MF@LP|Li cells are disassembled after cycling to further study the Li deposition behavior. **Fig. 3a** and **Fig. 3b** illustrate the surface morphology of the Li metal after cycling. It can be seen that the Li surface in Li|MP@LP|Li is rough and has several protuberance, which may indicate the formation of Li dendrites. In contrast, the surface of Li metal in Li|MF@LP|Li is relatively smoother, suggesting the uniform Li deposition.

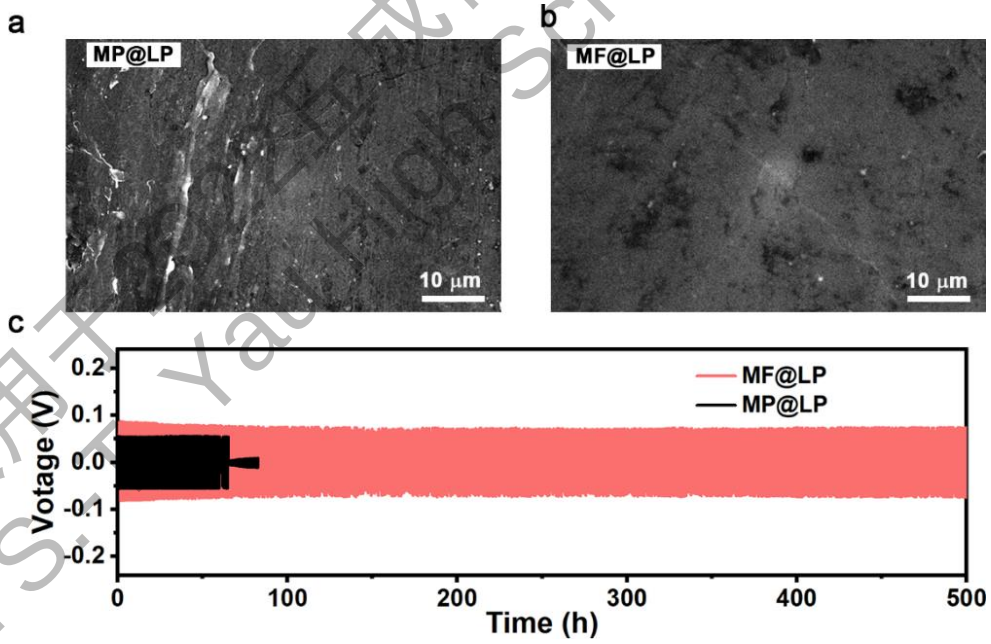

Figure 3. The SEM images of Li metal in (a) MP@LP and (b) MF@LP symmetrical batteries after cycling. (c) Long-term cycling stabilities of symmetric cells using MF@LP and MP@LP, respectively.

Full cells that using Li metal as anode and $LiFePO_4$ (LFP) as cathode have been assembled to evaluate the practical application of MF@LP as electrolyte. As shown in **Fig. 4a**, the Li | MF@LP | LFP delivered a high capacity of 157 mAh g^{-1}, and a high capacity retention of 145 mAh g^{-1} after 200 cycles at 0.5 C and 60 °C. The columbic efficiency is as high as 97 % during the cycling process, suggesting the high efficiency. In contrast, the Li | MF@LP | LFP suffers from a fast capacity decay from 150 to 127 mAh g^{-1} when its columbic efficiency decreases to about 84% after 39 cycles. The Li | MF@LP | LFP also shows a good rate performance, which achieves capacities of 164, 162, 157, 116 and 96 mAh g^{-1} at 0.2, 0.5, 1, 2 and 3 C, respectively (**Fig. 4b** and **4c**). When the current is back to 0.2 C, capacity of 163 mAh g^{-1} is recovered, verifying the high reversibility of the cell. The full cells are further cycled

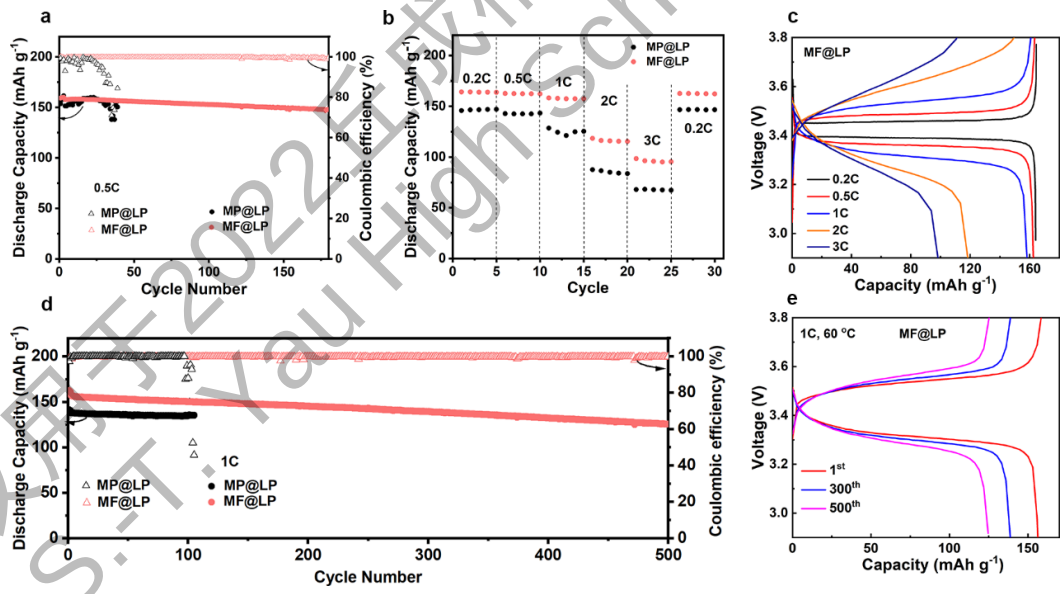

Figure 4. (a) Cycling performance of at 0.5 C and 60 °C. (b) Rate performance of Li | MF@LP | LFP and Li | MP@LP | LFP cells. (c) Charging/discharging curves of the full cells at 0.5 C. (d) Cycling performance at 1 C and 60 °C. (e) Charging/ discharging curves of MF@LP full cells at 1 C.

at 1 C to evaluate their cycling stability at high charging/discharging rate (**Fig. 4d** and **4e**). The Li|MF@LP|LFP battery can stably run for 500 cycles at 1 C, where a high capacity of 127 mAh g^{-1} is maintained. Besides, the charging/discharging curves displays a small polarization, confirming the high conductivity and small interface impedance of the MF@LP electrolyte. The performance of Li|MP@LP|LFP is much lower than that of Li|MF@LP|LFP, proving the advances of the 3D MOF-incorporated fibrous structure in elevating battery performance.

4. CONCLUSION

To sum up, a 3D MOF-incorporated fiber, as well as the fiber-reinforced SPE have been successfully prepared. As solid filler, the intrinsic characters of MOFs (e.g., high surface area, rich porosity, surface polarization, ordered channels, etc.) and the 3D fibrous nanostructures of MF can significantly accelerate ion migration, regulate Li deposition and enhance the mechanical strength. Consequently, the as-obtained fiber-reinforced MF@LP demonstrates high ionic conductivity, wide electrochemical window, and long cycling stability. When assembled into batteries, the MF@LP can stabilize the interfacial contact with electrode and inhibits Li dendrites growth. Both the Li symmetrical cell and full cell show excellent cycling stability. A high capacity of 127 mAh g^{-1} is maintained after 500 cycles at 1 C and 60 ºC. This work verifies the effectiveness of MOF-incorporated fibers in producing high-performance SPEs for advanced ASSBs.

References

[1] DUAN J, TANG X, DAI H, et al. Building Safe Lithium-Ion Batteries for Electric Vehicles: A Review[J]. Electrochemical Energy Reviews, 2020, 3(1): 1-42.

[2] LI M, LU J, CHEN Z, et al. 30 Years of Lithium-Ion Batteries[J]. Advanced Materials, 2018, 30(33): 1800561.

[3] FAN L, WEI S, LI S, et al. Recent Progress of the Solid-State Electrolytes for High-Energy Metal-Based Batteries[J]. Advanced Energy Materials, 2018, 8(11): 1702657.

[4] JANEK J, ZEIER W G. A solid future for battery development[J]. Nature Energy, 2016, 1(9): 16141.

[5] FAMPRIKIS T, CANEPA P, DAWSON J A, et al. Fundamentals of inorganic solid-state electrolytes for batteries[J]. Nature Materials, 2019, 18(12): 1278-1291.

[6] ZHONGLIANG LI S W. A 3D interconnected metal-organic framework-derived solid-state electrolyte for dendrite-free lithium metal battery[J]. Energy Storage Materials, 2022, 47: 8.

[7] RUO ZHAO Y W, ZIBIN LIANG, LEI GAO, WEI XIA, YUSHENG ZHAO AND RUQIANG ZOU. Metal-organic frameworks for solid-state electrolytes[J]. Energy & Environmental Science, 2020

Acknowledgments

I would like to express my sincerest gratitude to my volunteer instructor, Ms. Zhao (Ruo Zhao) from the Southern University of Science and Technology (SUSTech), who helped me to determine my topic, and design the experiments. I also want to pay special thanks to the generous support from Mr. Xu (Yifan Xu), a postgraduate student whom

I met in SUSTech. He volunteered to instruct my experiments and taught me many useful skills.

Last but not least, I really want to thank this experience of competing for the S. -T. Yau High School Science Award, from which I learned much more about the field I'm obsessed with, as well as gained many skills in scientific research. I also want to express my deepest gratitude to Ms. Yanfang Liu, who is my first chemistry teacher in junior high and greatly stimulated my interest in chemistry; as well as Mr. Ping Yang, my chemistry teacher in senior high, who helped me a lot in learning chemistry.